Numerical and experimental investigation of forming limit diagrams of 6063 aluminum alloy sheets using Ayada ductile fracture criterion and the second derivative of large strain criterion at increased temperatures

Abstract

The present study investigated the forming limit diagrams (FLDs) of aluminum alloy 6063 sheets using numerical and experimental methods at increased temperatures. In the numerical section, for the first time, the Ayada ductile fracture criterion and the second derivative of the large strain criterion were used. ABAQUS finite element (FE) analysis software was employed for the simulations. In order to determine necking time, after simulation, relevant data such as stress history, principal stresses, equivalent strain history, and large strain were extracted and the conditions for the necking criteria were investigated. To obtain the FLD in the experimental part, a Nakazima format was used. Experiments were conducted at temperatures of 25, 150, 200 and 250 degrees Celsius for the samples with equal lengths and different widths. Ayada criterion had better compatibility with the left side of the FLD (for small negative strains), while the second derivative of the large strain criterion had better compatibility with the right side of the diagrams (for small positive strains). The results also showed that with the increase in temperature, the FLD moved upward and sheet forming was improved. This improvement was almost similar for the temperatures of 150 and 200ºC, while the processing temperature of 250ºC led to significant improvement in forming, as compared to other temperatures.

Keywords

FLDs, FE analysis, aluminum alloy 6063, increased temperatures, Ayada ductile fracture criterion, second derivative of large strain criterion

Alireza Heidari[a,b]
Aazam Ghassemi[a,b]*
Amir Atrian[a,b]

[a] Department of Mechanical Engineering, Najafabad Branch, Islamic Azad University, Najafabad, Iran. E-mail: heidari_2002@yahoo.com, a_ghassemi@pmc.iaun.ac.ir, atrian@pmc.iaun.ac.ir

[b] Modern Manufacturing Technologies Research Center, Najafabad Branch, Islamic Azad University, Najafabad, Iran

*Corresponding author

1. Introduction

Predicting fracture and necking in sheet metals can be extremely difficult. Many studies have been recently carried out for the prediction of FLDs (See Appendix A) using ductile fracture criteria. Schey (1992) for instance, studied the improvement of production control by determining the formability of materials. Takuda et al. (1996) similarly, used the criterion in order to predict fracture initiation for the deep drawing process in the case of composite sheets. Overall, the findings have revealed successful predictions, concluding that using the ductile fracture criteria could be effective for low ductility materials. Takuda et al. (1999) employed a wide range of ductile fracture criteria. Brozzo et al. (1972) in order to simulate cylindrical deep drawing based on the finite element method (FEM). It was assumed that deformation was axisymmetric, while anisotropy was normal. The results obtained by the calculations exhibited good compatibility with the experimental results. Butuc et al. (2003) proposed a code to predict the FLD for any hardening law, yield function, or constitutive equation. This research, in fact, verified the theoretical study by an experimental test. Li and Ghosh (2004) on the other hand, addressed the biaxial warm forming behavior in the temperature range of 200–350 °C for three automotive aluminum sheet alloys, revealing that temperature had a considerable effect on formability. Banabic et al. (2004) also focused on the FLD theoretical model to evaluate the effect of the plastic anisotropy on the sheet metal formability. Also, the model was compared with the experimental data in the case of an aluminum alloy. Ozturk and Lee (2004) performed analyses of forming limits by employing ductile fracture criteria. This fracture prediction was found to be successful for the left side of the FLD diagram, while it did not perform well for the right side. They made use of new and modified ductile fracture criteria. Therefore, critical strains in FLD with 20, 25, 30, 35, 40 and 45% of thickness were determined using FE simulation. Comparing the results with the experimental ones showed that the left side of FLDs had better compatibility, as compared to the right side. Campos et al. (2006) on the other hand, investigated the forming limit curve (FLC) of AISI 304 stainless steel using Marciniak-Kuczynski (M-K) method. They evaluated

theoretical results experimentally and achieved a very good agreement. Allwood and Shouler (2009) utilized a method to predict FLDs in sheet metal forming processes on the basis of strains in the entire working thickness. Since FLDs are dependent on strain path, the FLD does not affect analysis of complex processes. Stoughton and Yoon (2011) conducted a review of theoretical models for FLD based on strain and their relations to FLD based on stress, showing that FLDs based on stress in all forming processes depended on strain path. Mixing variables such as equivalent plastic strain, tensile stress and hydrostatic stress is needed for fracture evaluation based on uncoupled criteria; these are related to fracture initiation and propagation Wierzbicki et al. (2005). Wu et al. (2009) showed that ductility of materials was increased with hydrostatic stresses, such that in most uncoupled criteria, it could be observed that this stress affected fracture initiation or propagation. Yue et al. (2015) addressed the formability of aluminum alloy AL7020 nu employing FLD, forming limit stress diagram (FLSD) and coupled constitutive equations, considering the mixed nonlinear isotropic and kinematic hardenings fully coupled with the isotropic ductile damage. The results have been evaluated by Nakazima test.

Ayada et al. (1987) on the other hand, suggested a ductile fracture criterion which was based on the effect of stress triaxiality and the equivalent plastic strain on the fracture states.

Min et al. (2010) probed the influence of necking types on the left-hand side of the FLD. Likewise, Mitukiewicz et al. (2014) addressed the left side of FLD via gas blow forming. Later, Khan and Liu (2012) developed a new empirical criterion which was based on the stress vector criterion. Khan and Huang (1995) on the other hand, employed the hydrostatic stress and the stress vector value, showing that this criterion could more accurately predict ductile fractures under various deformations, in comparison to criteria proposed by people such as Xue (2008). Liu and Fu (2014) also managed to improve the Ayada ductile facture criterion according to the effects of stress triaxiality and equivalent plastic strain on the results. Accordingly, the performance and reliability of the ductile fracture criteria for predicting both stress situations, which included sheer and tensile stress, in sheet metal forming were investigated. That study also probed the deformation behaviors and fracture in Al6061 and Ti0A materials, showing that experimental data and simulation results had suitable reliability for this criterion.

The use of fracture criteria is essential to analyze simulation results in the onset of necking. Brun et al. (1999) addressed thinning of sheet metals by employing the Nakazima method to determine the necking onset. Geiger and Merklein (2003), by utilizing the same test, found that during the onset of necking, the major strain gradient was changed quickly. Narasimhan (2004) tried to predict the onset of necking by using limit drawing height (LDH) test and considering the thickness strain gradient in the surrounding areas. Zadpoor et al. (2007) also aimed to improve the M-K model by utilizing FE simulation in ABAQUS software, showing that mixing the M-K model with Storen-Rice analysis could lead to the prediction of dome height with good accuracy. Petek et al. (2005) based on the Marciniak test, suggested a new method to evaluate thickness strain as a function of time and the first and second derivatives of the thickness strain. Accordingly, the maximum point of the second derivative of thickness strain vs time was found to show the onset time of necking. Volk (2006) used experimental tests and numerical simulations to propose a new method for detecting necking. By using the calculated strain rate, detection was carried out with two important effects. In the necking localization, the number of necking points was increased with strain rate, leading to the reduction in strain rate outside the necking area.

Zhang et al. (2009) performed numerical and theoretical studies regarding the effects of strain change rates on the forming abilities of AA5083 alloy. In their work, the behavior of the aluminum alloy was investigated at high temperatures. They used the Swifts' hardening law in order to explain the visco-plastic behavior and the M-K model and the Marciniak test to crease FLDs and address the effects of the rate sensitivity index on forming capabilities. According to the FEM results, various fracture criteria were employed to determine the necking location. FLDs in 150, 240 and 300 degrees Celsius were determined and the results showed that with the increase in temperature, the forming capability of this alloy was improved.

Aluminum alloys are often employed in such industries as automobile and aerospace owing to their good corrosion resistance and moderate weld ability, as well as high ultimate strength. Formability of aluminum sheets at room temperate is moderate. However, with the increase in temperature, the formability of aluminum sheets and the possibility of creating more complex parts are increased. Warm forming is a process during which metal sheets are formed at temperatures higher than 150ºC, but below their recrystallization temperature. In this temperature range, ductility of aluminum alloys is greatly improved and their flow resistance is decreased (Abedrabbo et al. (2007)).

Various studies by Shehata et al. (1978) have been conducted on series 5000 aluminum (AA5005 and AA5082) using the uniaxial tensile stress test and the punch stretching test. They observed that at temperatures below 300ºC, elongation of these alloys was decreased with the increase in temperature and at low strain rates. Naka and Yoshida (1999) studied a special type of serried 5000 aluminum (AA5083). Their study concentrated on deep draw ability of sheets at different speeds and temperatures between 20 to 180ºC. They observed that with the increase in the temperate of die and punch, the limit drawing ratio (LDR) was increased and that this parameter was decreased with the increase in the drawing speed at all temperatures. Bolt et al. (2001) studied different types of aluminum alloys (1050-H14, 5754-O

and 6016-T4) in the temperature range of 100-250ºC. Takuda et al. (2002) performed a deep tensile test on AA5182-O alloy. Their results showed that in order to reach a higher LDR, temperature related flow stress should be distributed uniformly along the entire sheet.

Kim et al. (2006) determined the FLDs Al5182+Mn sheets at 250, 300 and 350ºC. In their study, a set of parameters including maximum load, minimum thickness and thickness ratio were employed for the optimization of the fracture initiation criterion. Their model managed to predict that the high temperature gradient between die and punch resulted in better formability.

Kaya et al. (2008) performed a series of studies on the deep draw ability of AA5754-O, AA5052-H32 and AZ31B-O alloys in constant temperatures in the die and punch set and different speeds. In this study, the die temperature was set to 310ºC, while the punch had the temperature of 65ºC, and the maximum punch speed for aluminum and magnesium alloys was 35 mm/s for 300ºC and 300 mm/s for 275ºC, respectively. They concluded that the increase in temperature led to thinning of the cup bottom for aluminum alloys, but this phenomenon was not observed in magnesium alloys.

Bagheriasl et al. (2014) in several works in 2014 studied the isothermal warm formability of AA3003 aluminum alloy. They drew the FLDs at different temperatures (room temperature, 100, 200, 250 and 300ºC) and calculated different strain rates. In their studies, it was observed that sheet formability was improved significantly with the increase in temperature, and that forming speed has a small effect on sheet formability.

Dicecco et al. (2016) determined the FLD of AA6013-T6 aluminum alloy using the localized necking criterion. In their work, the forming limit behaviors of aluminum alloy sheets were investigated under isothermal conditions at room temperature and 250ºC by using the LDH test. Their results showed that at 250 ºC, the limiting strains generated by using the necking zone approach were 31-34% larger than ISO strains developed under plane strain and biaxial loading conditions.

Bressan et al. (2016) attempted to model the forming limit strains of AA5083 aluminum alloy at room and high temperatures (400 ºC). Accordingly, a novel mathematical model was suggested to predict the necking onset and fracture initiation. The results showed that the formability of AA5083 alloy was increased significantly at elevated temperatures, as compared to that at room temperature. In this study, they also introduced a new concept called ductile fracture using sheer stress, and its M-K model had good compatibility with Bressan-J.D models. Based on various studies, it seemed that predicting fracture in aluminum alloys could be of great importance, especially at elevated temperatures.

In this study, first, the history of equivalent strain, large strain, stress and principal stresses for critical elements with the largest strain was extracted; then, the Ayada criterion was used for the numerical integration of equation (1). When the integral results became equal to a constant value for each equation, the time was determined as the necking onset time. This constant value was calculated using the numerical integral solution of each equation for the uniaxial drawing graph. This was repeated for different strain paths (different geometries) at different temperatures (25, 150, 200 and 250 ºC), and the FLDs were determined using the Ayada ductile fracture criterion.

To determine the strain limits using the maximum of largest strain acceleration method, after selecting the suitable element which had the largest strain in the analytical model, the history of the largest strain over time was extracted and large strain rate graphs (the first derivative of the large strain over time) were determined. Then, the large strain acceleration graph (the second derivative of the large strain over time) was calculated. When the large strain acceleration reached its maximum value, the moment of necking onset, and large (ε_1) and small (ε_2) strains (Major and Minor strain) at this moment were strain limits. By repeating this process for different strain paths and changes in geometry and different temperatures, it was possible to determine the strain limits for the entire range of forming limit graphs at different temperatures.

2. Materials

The aluminum alloy used in the present study was the type AA6063. , Its chemical composition was determined using Quantometry method, as presented in Table 1, based on weight percent.

Table 1: Chemical composition of AA6063 aluminum alloy based on weight percent of elements

Al	Mg	Si	Fe	Zn	Cu	Mn	Pb	Ti	Ni	Sn	Gn
Base	0.47	0.44	0.30	0.08	0.06	0.03	0.03	0.03	0.02	0.02	0.01

To determine the mechanical properties of sheets, the study employed the uniaxial tensile strength test. A schematic of uniaxial tensile strength test equipment is shown in Figure 1. As can be seen, this equipment included a furnace and the first sample was attached between the upper and lower claws; it was then placed within the furnace. In order to perform the uniaxial tensile strength test, furnace temperature was increased and the actual temperature was determined using a temperature sensor inside the furnace and recorded in the attached computer. With the increase in furnace and therefore, sample temperature, after reaching a predetermined temperature, temperature remained constant and the claws

started to move. Finally, the stress – strain graphs of the samples for different temperatures were extracted, as shown in Figure 2. Samples were prepared using wire cutting in accordance with the ASTM E08 standard in order to prevent residual stress in samples.

Figure 1: Schematic of tensile strength test equipment
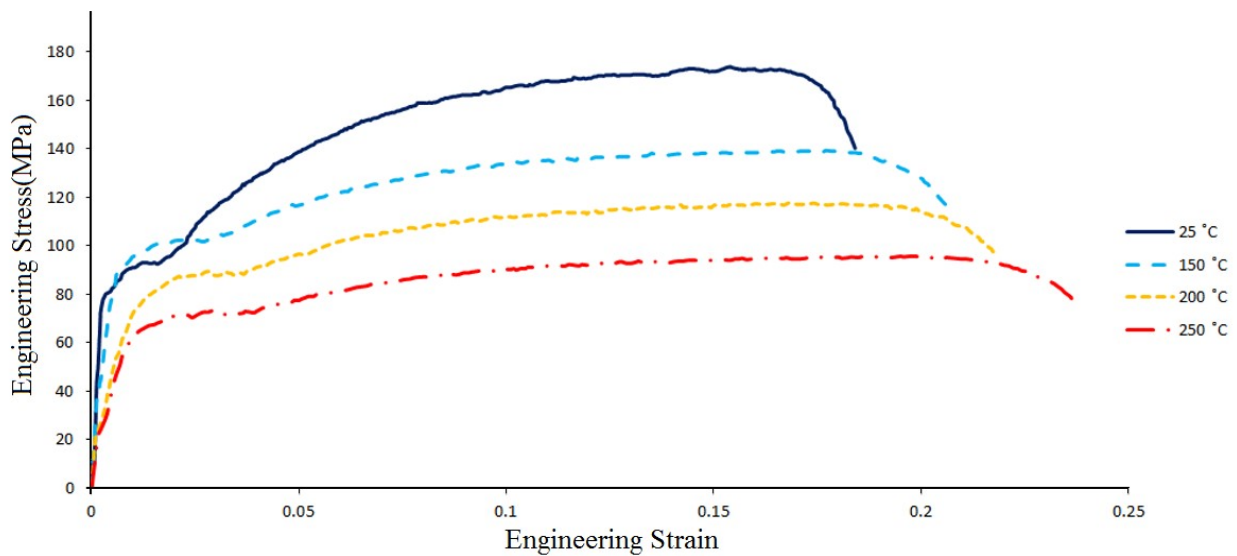
Figure 2: Stress – strain graph of AA6063 aluminum alloy at different temperatures

A total of five Aluminum-AA6063 samples with different widths of 45, 60, 75, 90 and 105 millimeters, the constant length of 105 mm, and the thickness of 1 mm were used for the forming limit tests. Electrochemical etching method was used for latticing samples' surfaces. Samples which were used for Nakazima out of plate tensile tests are shown in Figure 3.
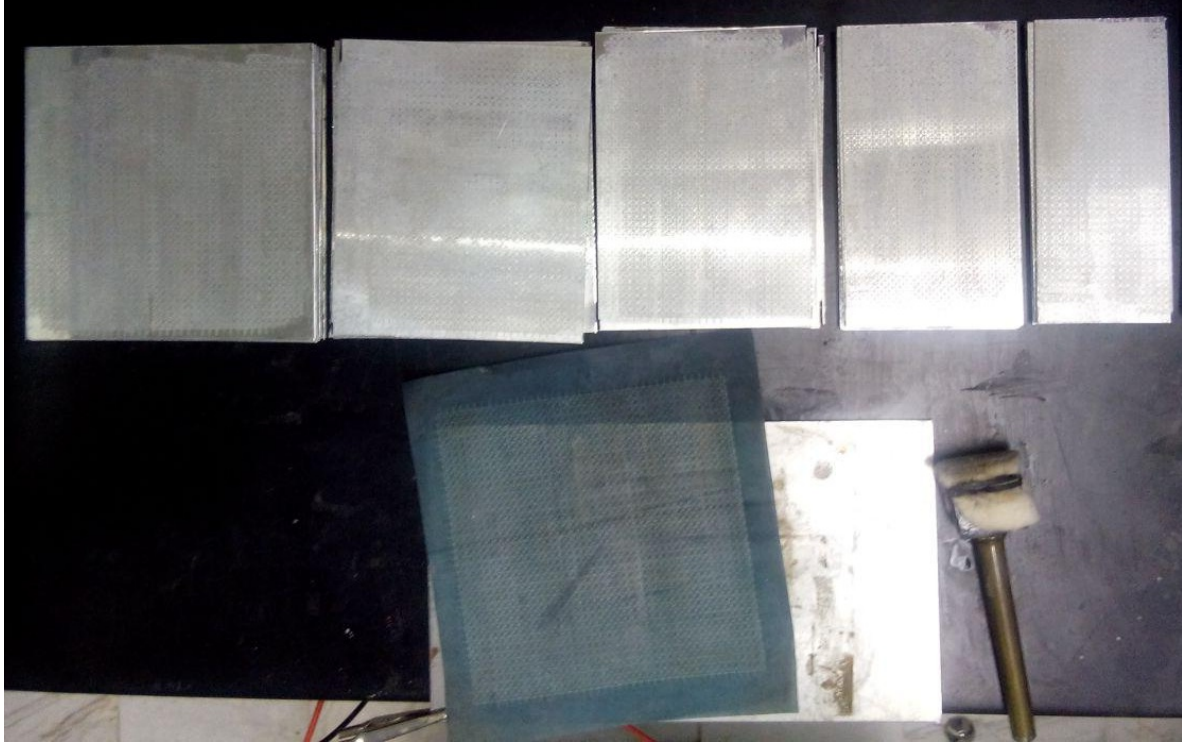
Alireza Heidari et al.
Numerical and experimental investigation of forming limit diagrams of 6063 aluminum alloy sheets using Ayada ductile fracture criterion
and the second derivative of large strain criterion at increased temperatures

Figure 3: Nakazima test samples

3. Finite element analysis

In order to determine the formability of the aluminum sheet, ABAQUS / Explicit FE software was used. 3-dimensional FE model of the Nakazima test is shown in Figure 4. The sheet was simulated as a 3-dimentional, deformable and homogeneous part. The punch, the holder, and the matrix were modeled as a discrete rigid body. The temperature distribution was uniform among the whole sheet. The matrix was fixed and the holder and the punch were allowed to move in the z-axis of the punch. Since sheets were tested at different temperatures; for defining sheet characteristics at different temperatures, the strain-stress graph extracted in the same temperature was used.
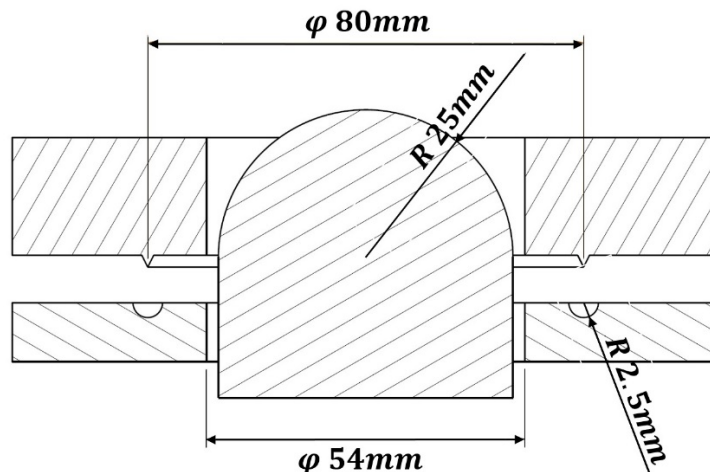
Figure 4: Schematic of the die used

For the simulation of the process, two steps including clamping and drawing were defined. In the first step, the clamp was tangent to the sheet's surface, moving downward, and the sheet was fully attached to the matrix so that it would remain completely stationary during the process and could not slip inside the matrix. In the next step, the punch moved upward, forming the sheet. In both steps, no forces were applied to clamp and punch and the process was fully

Alireza Heidari et al.
Numerical and experimental investigation of forming limit diagrams of 6063 aluminum alloy sheets using Ayada ductile fracture criterion
and the second derivative of large strain criterion at increased temperatures

defined based on the actual process with controlled displacement and constant speed, as fully explained in the experimental section. In order to investigate the strain path, the samples were modeled in five different geometries and each geometry was evaluated at different temperatures.

The material properties of the sheets using in FE simulation are presented According to the following specifications

Material : Aluminum AA6063

Density : 2780 kg/m^3

Young Module (E) : 69 GPa

Poisson ratio : 0.33

In order to define plastic behavior, the results of the uniaxial tensile test were used. So the stress-strain engineering diagram (Fig. 2) was extracted from the force- displacement graph; then, by the plasticity formulation, the true stress-strain diagram was extracted from it and the plastic properties of that graph were defined for the software in order to do the analysis

The interaction between the punch and the sheet surfaces was defined using the penalty contact method. The friction coefficient was considered to be 0.1 between the punch and the sheet. Due to the high velocity of the forming process, the heat did not have enough time to dissipate and therefore, the temperature inside the sheet was assumed to be fixed; as a result, the FE simulations were performed mechanically, without considering the thermal effects. The model was symmetric and therefore, a quarter of it could be simulated to have less computational costs

After the simulation was done, the history of stress and strain was investigated in the critical element and the necking point was determined using the Ayada ductile fracture and the maximum large strain acceleration criteria.

For example Von Mises Stress (S.Mises) and Equivalent Plastic strain (PEEQ) distributions are graphically shown for a sample with the width of 45 mm in Figure 5.
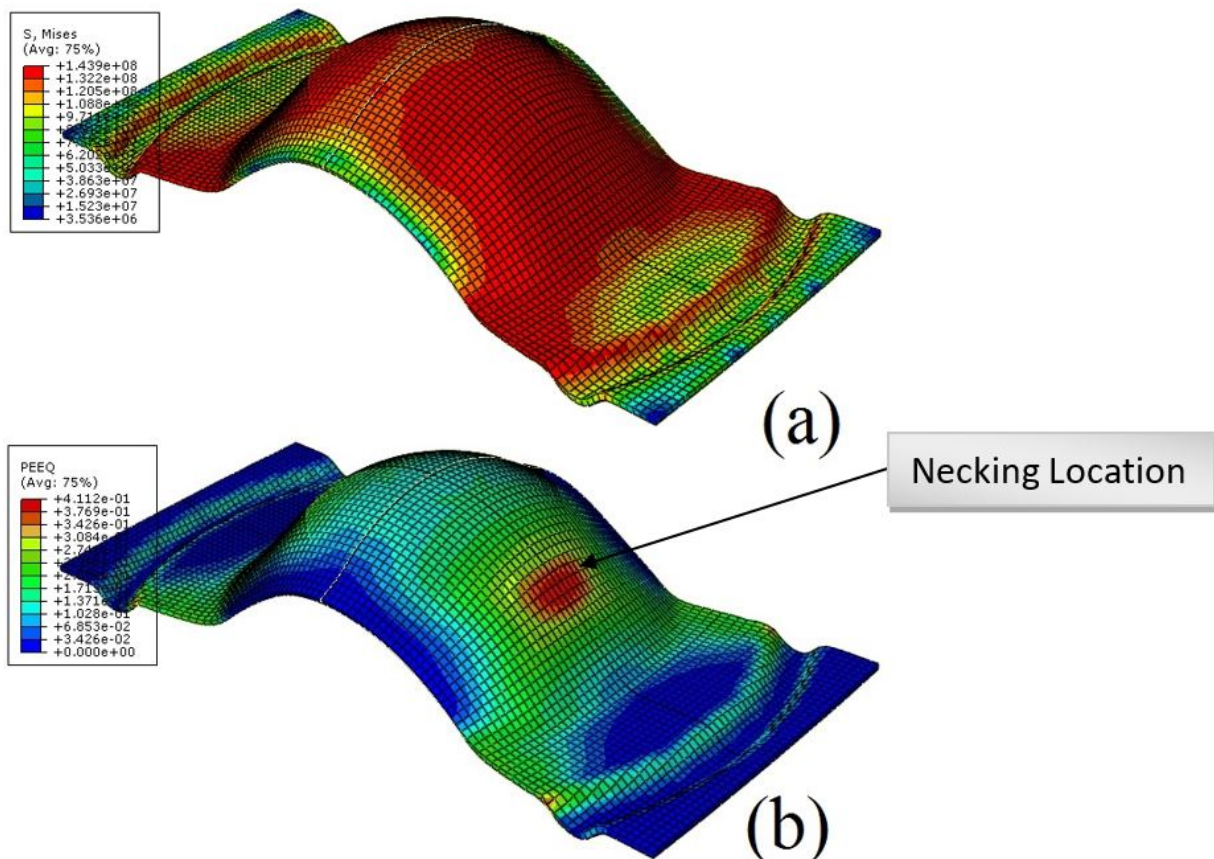
Figure 5: *Graphical representation of (a) Stress distribution and (b) Strain distribution*

To probe the effect of FE analysis sensitivity to mesh size, the simulation process was carried out for the sample with the mesh size of 4, 3, 2, 1 and 0.1mm, and the maximum force applied on the punch for all five conditions was extracted. The results showed that the mesh size 1 mm was the optimum mesh size. Figure 6 shows graph's sensitivity to mesh size. As can be seen in this graph, with the decrease in the mesh size from 4mm to 1mm, the force applied on punch was also decreased and finally, with the change from 1mm to 0.1mm in mesh size, the force showed a reverse behavior and increased.

Alireza Heidari et al.
Numerical and experimental investigation of forming limit diagrams of 6063 aluminum alloy sheets using Ayada ductile fracture criterion
and the second derivative of large strain criterion at increased temperatures

As a result, according to Figure 6, in the range of 0.5 mm to 1 mm, the size of the mesh does not give rise to any specific changes in the results, and there is no mesh sensitivity in this range. So, to have the appropriate time, speed and volume for the estimations, we use the mesh size of 1 mm.
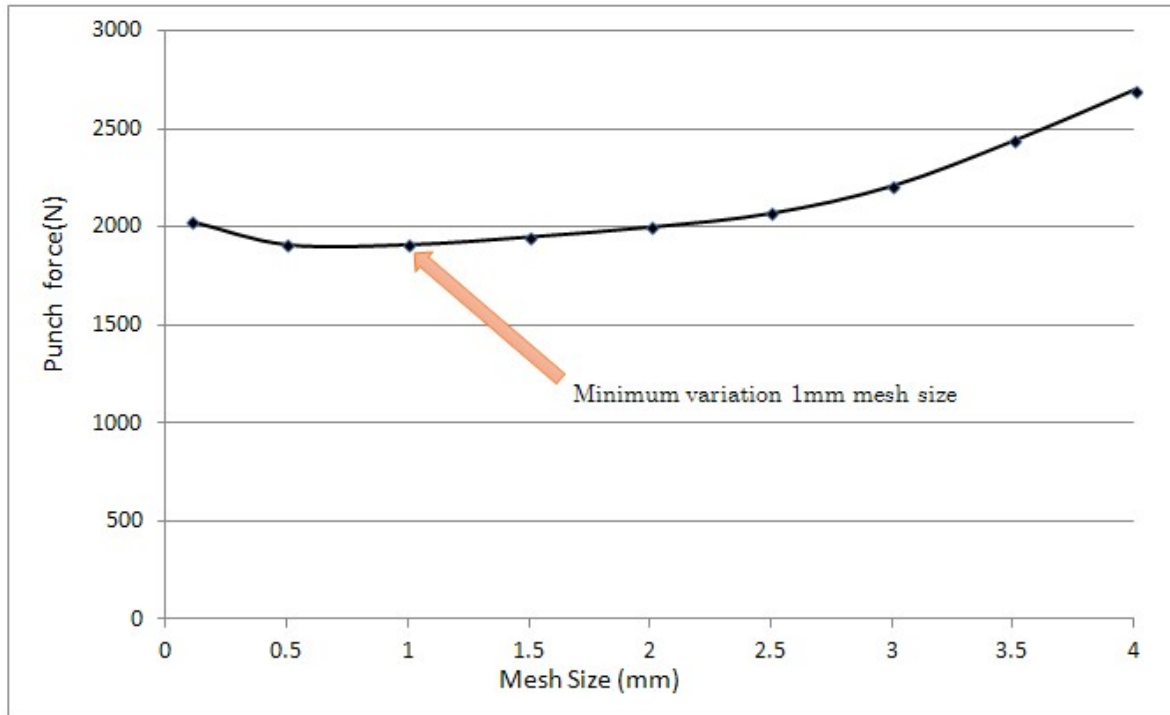

Figure 6: *Graph showing sensitivity to mesh size*

After the implementation and completion of the simulation process, the most important step is to analyze the obtained data, such as the history of the types of stresses and strains, so that a logical relationship between them and the beginning of necking can be established. To find the FLD of a metal sheet by FE simulation, it is important to determine a criterion for the prediction of the moment of necking to ensure the accuracy of the FLD obtained for us.

The failure criteria used in the FE simulation for plotting the FLD chart are:

3.1. Ayada ductile fracture criterion

The Ayada criterion was chosen because it is a reliable one for predicting the formability of the sheet used with a low error (Ayada et al. (1987)).

In order to determine strain limits using the Ayada ductile fracture criterion, the effect of average stress was investigated. This criterion is shown using Equation (1).

$$\int_0^{\bar{\varepsilon}_f} \frac{\sigma_m}{\bar{\sigma}} d\bar{\varepsilon} = C_1 \tag{1}$$

Here, $\bar{\sigma}$ is the effective stress (von Mises stress), and σ_m is the average stress (Hydrostatic stress) that can be calculated by using Equation (2):

$$\sigma_m = \frac{\sigma_1 + \sigma_2 + \sigma_3}{3} \tag{2}$$

In this Equation, σ_1, σ_2 and σ_3 are principal stresses and C_1 is the critical value of the Ayada criterion in uniaxial tensile test, and $\bar{\varepsilon}_f$ is the effective strain when fracture occurs

At elevated temperatures, C_1 changes, and depending on the process temperature.

The average stress is equal to one third of effective stress in uniaxial tensile test (Equation (3)).

$$\sigma_m = \frac{1}{3}\bar{\sigma} \tag{3}$$

By inserting Equation (3) in Equation (1) in the uniaxial tensile test, Equation (4) is obtained.

$$\int_0^{\bar{I}_f} \frac{\frac{1}{3}\bar{\sigma}}{\bar{\sigma}} d\bar{I} = C_1 \rightarrow \frac{1}{3}\int_0^{\bar{I}_f} d\bar{I} = C_1 \rightarrow \frac{1}{3}\bar{I}_f = C_1 \qquad (4)$$

The steps in drawing the FLD in the Ayada ductile fracture criterion are as follows.

In the first step, after performing a uniaxial tensile test and obtaining the results of the true stress and strain data obtained from the above test, by measuring one-third of the plastic strain at the moment of fracture, the value C_1 is calculated according to the Equation (4).

These constant values were calculated of the above equation for the uniaxial tensile test graph, at different temperatures, as presented in Table 2. (The constant value is equal to one third of The effective strain when fracture occurs)

Table 2: Constant values calculated by numerical integration of Equation (1) for uniaxial stress-strain graph at different temperatures

T	25°C	150°C	200°C	250°C
C_1	0.057	0.063	0.07	0.079

In the second step, to determine the critical element in the simulated model, the File output mode in the software is in peeq one and by using the report, the critical element number is determined. (the element that has the highest peeq is the critical element). Then, the data on the history and the stresses and strains of the parameters with time, eqivalent Plastic strain(peeq), maximum principal strain$\left(pe_{max.principal}\right)$, mid principal strain($pe_{mid.principal}$) , von mises stress (s_{mises}), maximum principal stress$\left(s_{max.principal}\right)$, mid principal stress($s_{mid.principal}$), minimum principal stress $\left(s_{min.principal}\right)$, average stress($s_{ave}$) are obtained. ($s_{ave} = \frac{s_{max}+s_{mid}+s_{min}}{3}$)

For the critical element mentioned, the simulation results are used. by putting $\bar{I}_f = peeq, \sigma_m = s_{ave}, \bar{\sigma} = s_{mises}$ in equation (1) for all intervals of process times, the result of the integral of the above equation is obtained. For the time data in which the values obtained from the integral were equal to the value obtained from the uniaxial tensile test (C1), the time was taken as the necking time of the sheet; at that time, the parameters $pe_{max.principal}, pe_{mid.principal}$ respectively, are taken as Major(ε_1) and Minor(ε_2) strains.

For example, the data related to the above parameters, along with the calculation of Major (ε_1)) and Minor(ε_2) strains for sheets with a width of 45 mm and a temperature of 25 ºC are given in Table 3.

This process was repeated for different strain paths (different geometries) at temperatures of 25, 150, 200 and 250ºC; then FLDs were determined using the Ayada ductile fracture criterion.

Alireza Heidari et al.
Numerical and experimental investigation of forming limit diagrams of 6063 aluminum alloy sheets using Ayada ductile fracture criterion
and the second derivative of large strain criterion at increased temperatures

Table 3: *Simulation results for sheet samples with a width of 45 mm and a temperature of 25 ºC (Ayada criterion)*

time(s)	peeq	pe max	pe mid	s mises (Pa)	s max (Pa)	s mid (Pa)	s min (Pa)	s average (Pa)	ayada criterion $C_1 = 0.057$
0	0	0	0	0	0	0	0	0	0
0.25	0	0	0	2.05E+07	1.67E+07	6.45E+05	-6.42E+06	3635640	0.00E+00
0.5	0	0	0	3.42E+07	2.83E+07	4.57E+05	-9.86E+06	6295967	0.00E+00
0.75	0.00E+00	0.00E+00	0.00E+00	7.42E+07	6.51E+07	-1.46E+05	-1.55E+07	16493416	0.00E+00
1	7.24E-06	7.14E-06	-2.56E-06	6.49E+07	5.81E+07	1.18E+05	-1.19E+07	15467998	0.00E+00
1.25	7.24E-06	7.14E-06	-2.56E-06	3.78E+07	2.88E+07	-1.25E+06	-1.36E+07	4644550	0.00E+00
1.5	7.24E-06	7.14E-06	-2.56E-06	2.76E+07	1.66E+07	-5.42E+05	-1.52E+07	289818.7	0.00E+00
1.75	7.24E-06	7.14E-06	-2.56E-06	1.88E+07	7.39E+06	-1.92E+05	-1.40E+07	-2268242	0.00E+00
2	7.24E-06	7.14E-06	-2.56E-06	1.54E+07	2.37E+06	-1.12E+06	-1.45E+07	-4416190	0.00E+00
2.25	7.24E-06	7.14E-06	-2.56E-06	2.70E+07	1.29E+07	-1.42E+06	-1.83E+07	-2273523	0.00E+00
2.5	7.24E-06	7.14E-06	-2.56E-06	4.88E+07	3.53E+07	-1.82E+06	-1.99E+07	4515497	0.00E+00
2.75	7.24E-06	7.14E-06	-2.56E-06	6.17E+07	4.66E+07	-2.20E+06	-2.29E+07	7170953	0.00E+00
3	7.24E-06	7.14E-06	-2.56E-06	7.09E+07	5.39E+07	-2.62E+06	-2.56E+07	8577790	0.00E+00
3.25	0.000123	0.000118	-2.69E-05	7.97E+07	5.94E+07	-2.32E+06	-3.05E+07	8879410	1.30E-05
3.5	0.000872	0.000842	-0.00023	8.24E+07	6.87E+07	-1.90E+06	-2.18E+07	15020660	1.49E-04
....	....	....	....	....	....	....	....	....	....
8.5	0.164124	0.163735	-0.0804	1.81E+08	1.90E+08	1.95E+07	8.86E+05	70207863	5.42E-02
8.75	0.180444	0.179952	-0.08982	1.83E+08	1.96E+08	2.77E+07	6.14E+05	74632077	6.08E-02
9	0.199529	0.198853	-0.09706	1.83E+08	1.98E+08	3.26E+07	1.36E+06	77285877	6.89E-02
9.25	0.226604	0.225459	-0.10609	1.83E+08	2.01E+08	4.76E+07	-1.12E+06	82583497	8.11E-02
9.5	0.261054	0.258881	-0.11565	1.83E+08	2.00E+08	5.40E+07	-4.66E+06	83261490	9.68E-02
9.75	0.318989	0.313525	-0.12642	1.83E+08	2.09E+08	7.32E+07	5.73E+05	94169685	1.27E-01
10	0.425971	0.412069	-0.13985	1.83E+08	2.16E+08	9.57E+07	5.57E+06	1.06E+08	1.88E-01

Ayada criterion: ε_1 (major strain) $= 0.165$, ε_2 (minor strain) $= -0.0825$

3.2. Second derivative of the large strain criterion

Situ et al. (2011) selected the maximum Second derivative (acceleration) of the large strain as the criterion for necking in metal sheets.

The steps in drawing the FLD for the maximum acceleration (second derivative) of the large strain are as follows.

In the first step, after determining the critical element, as described above, and obtaining the simulation results, including the maximum principle strain $\left(pe_{max.principal}\right)$ parameter data for the critical element, the history of the large (major) strains is extracted in terms of time. For example, the table related to data and the graph of the above parameter for a sheet with a width of 45 mm and a temperature of 25 ºC are shown respectively in Table 4 and Figure 7.

Table 4: *History of the major strain*

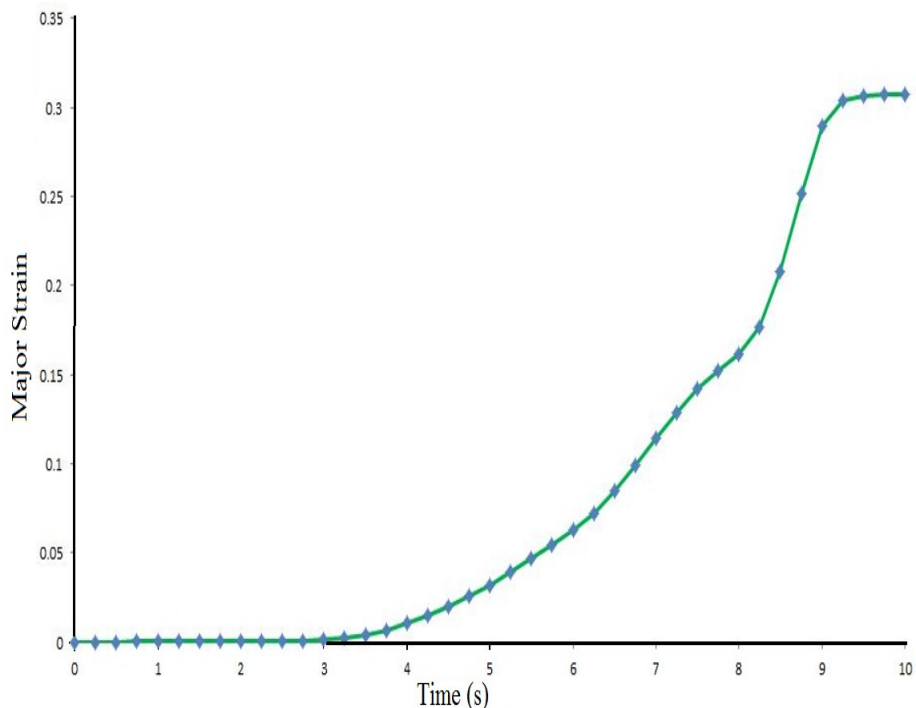| Time(s)	$pe_{max.principal}$ (Major Strain)
0	0
0.25	0.001445
0.5	0.001446
0.75	0.002896
1	0.002892
1.25	0.001446
....	....
8	0.16343
8.25	0.176446
8.5	0.208264
8.75	0.251653
9	0.290702
9.25	0.303719
9.5	0.306612
9.75	0.308058
10	0.308058

Figure 7: *Diagram of the major strain over time*

After extracting the history of the strains, in order to obtain the second derivative, the differentiate(x) operator in software is selected twice sequentially from the maximum principal strain(pemax. principal) parameter. Diagram of the first derivative of the major strain over time is shown in Figure 8. The table of data and the second derivative diagram of the major strain relative to the time for the above example can be obtained respectively according to Table 5 and Figure 9.
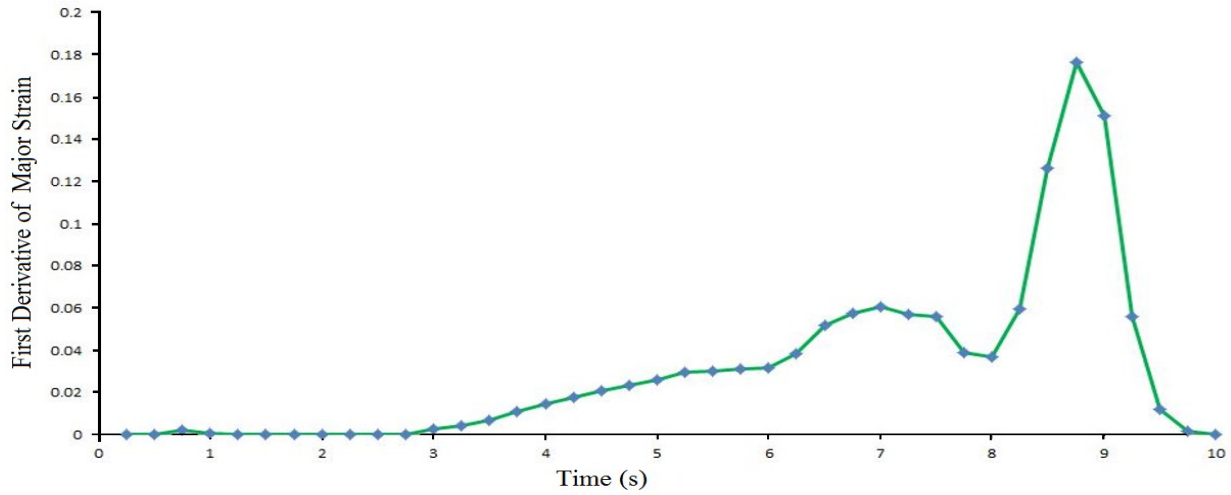
Numerical and experimental investigation of forming limit diagrams of 6063 aluminum alloy sheets using Ayada ductile fracture criterion and the second derivative of large strain criterion at increased temperatures

Figure 8: Diagram of the First derivative of major strain over time

Table 5: History of the Second derivative of major strain

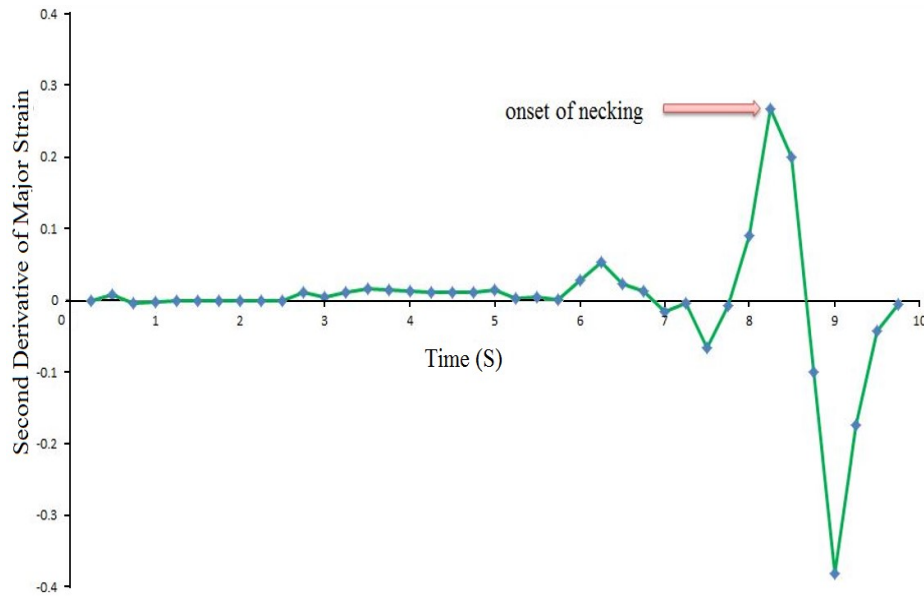| Time (s)	Second derivative of major strain
0	0
0.25	0
0.5	0.0086
0.75	-0.0043
1	-0.0021
1.25	-0.0023
....	....
8	0.0891
8.25	0.2652
8.5	0.2021
8.75	-0.1
9	-0.3804
9.25	-0.1767
9.5	-0.0434
9.75	-0.0043

Figure 9: Diagram of the Second derivative of major strain over time

In the second step, according to the Table 6, the moment when the second derivative of the major strain reaches its maximum is taken as the time of the start of necking, and at that moment, the strain value is determined from data (or diagram) of the major strain history. This strain represents the Major Strain (ε_1).

Table 6: History of the major strain and the second derivative of it (second derivative of large strain criterion)

(Major Strain) $pe_{max.principal}$	Time (s)	Second derivative of major strain
0	0	0
0.001445	0.25	0
0.001446	0.5	0.0086
0.002896	0.75	-0.0043
0.002892	1	-0.0021
0.001446	1.25	-0.0023
....	....	....
0.16343	8	0.0891
$\varepsilon_1(major\ strain) = 0.176446$ ⟵	8.25 ⟵	0.2652 (MAX)
0.208264	8.5	0.2021
0.251653	8.75	-0.1
0.290702	9	-0.3804
0.303719	9.25	-0.1767
0.306612	9.5	-0.0434
0.308058	9.75	-0.0043
0.308058	10	

By repeating the same procedure for the second derivative of the minimum principal strain $\left(pe_{min.principal}\right)$ parameter and by choosing the time data for the minimum derivative of the second small (minor) strain, the Minor Strain (ε_2) is also specified. By repeating the first and second steps for all samples at different temperatures, it is possible to determine the strain limits for the whole range of the FLD and then plot the FLD graph.

4. Experimental tests

For out of Nakazima plate tensile strength test, a 30-ton hydraulic press was employed. All experiments were conducted with the constant speed of 2 mm/s. At the beginning of the test, the sample was placed between the matrix and

Alireza Heidari et al.
Numerical and experimental investigation of forming limit diagrams of 6063 aluminum alloy sheets using Ayada ductile fracture criterion
and the second derivative of large strain criterion at increased temperatures

clamp. First, the clamp was moved downward, fully encompassing the sample. Then the punch was continued to move until a tear was formed. Figure 10 shows the die-punch set used in this study.
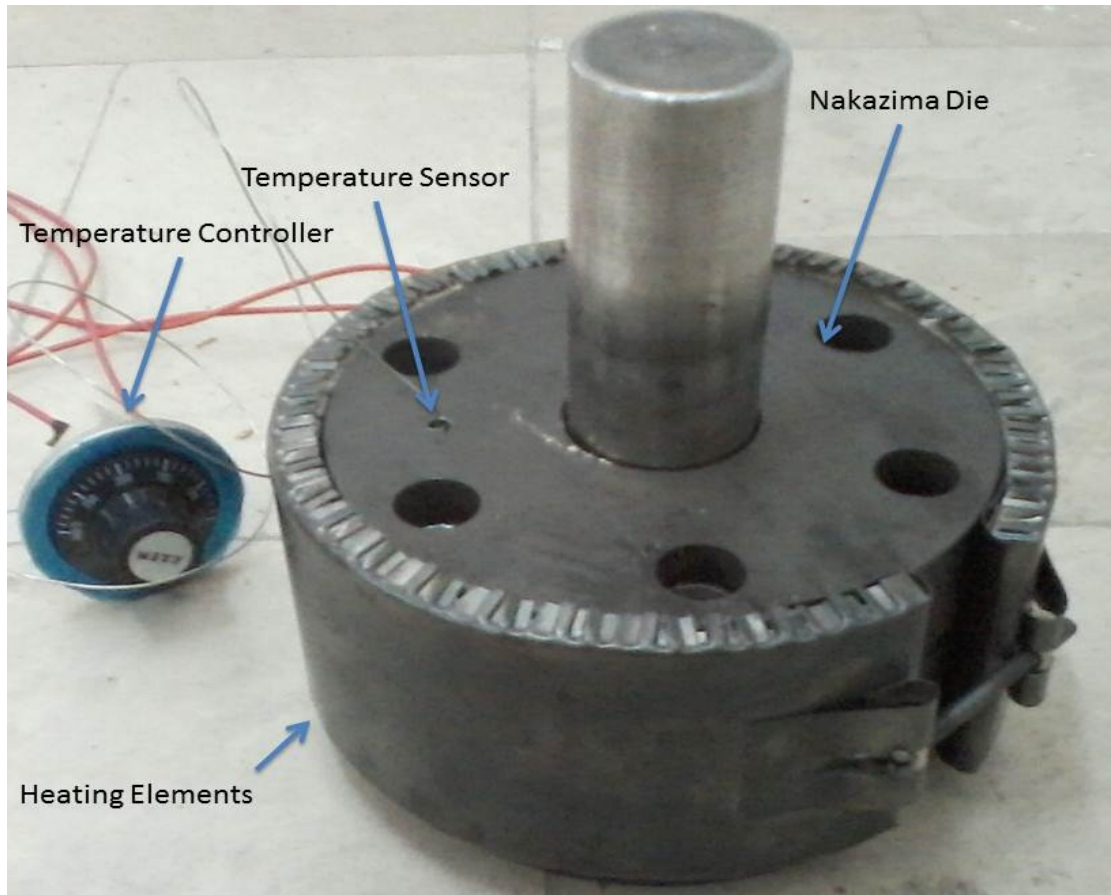

Figure 10: *The die-punch set used for experiments*

All experiments continued until necking or tear onset, when the process was stopped and strains were measured near the necking area and a distance of around 1.5 times of circle's diameter from fracture location was reached. After forming, circular lattices were turned into oval shapes in which the created engineering strains were measured using a microscope along with a caliper and employing true strains to measure the major (ε_1) and minor (ε_2) true strains, respectively. ε_1 And ε_2 of the samples are the x and y coordinates of the points used for creating the FLD. By repeating this process for all samples and determining the strain limits, FLDs were created.

Figure 11 shows the callipered microscope. During strain measurements, the line of sight was perpendicular to the investigated surface. By repeating this process for all samples and determining the strain limits, FLDs were created.

Alireza Heidari et al.
Numerical and experimental investigation of forming limit diagrams of 6063 aluminum alloy sheets using Ayada ductile fracture criterion
and the second derivative of large strain criterion at increased temperatures

Figure 11: *Callipered microscope used in experiments*

5. Results

The tear location of the sample in the experimental tests and FE analysis is shown in Figure 12. As can be seen, the tear location was near the center of the sample. There were also similarities between tear location in the experimental sample and the numerical analysis sample according to the Second derivative of large strain criterion.

The figures on the left show the distribution of the principal strain in the simulated models at the necking (or rupturing) time. As it is known, the geometric position of the maximum value of the principal strain is located at a close distance from the peak, which is in accordance with the geometric rupture and necking geometry shown in the right figures (experimental examples). It is necessary to explain that because the dimensions of the simulated sample (in part A of the above figure) were chosen in a square (105 mm × 105 mm), then in the simulation process of the Nakazima test, the model is under biaxial tension; and in this case, the highest strain is close to the peak of the sheet and in the periphery (red area). In addition, if the sample sheet is considered rectangular, its simulated model is in accordance with the section B (uniaxial tension) of Figure 12. This is the same confirmation of the results of the simulation of finite elements.

Alireza Heidari et al.
Numerical and experimental investigation of forming limit diagrams of 6063 aluminum alloy sheets using Ayada ductile fracture criterion
and the second derivative of large strain criterion at increased temperatures
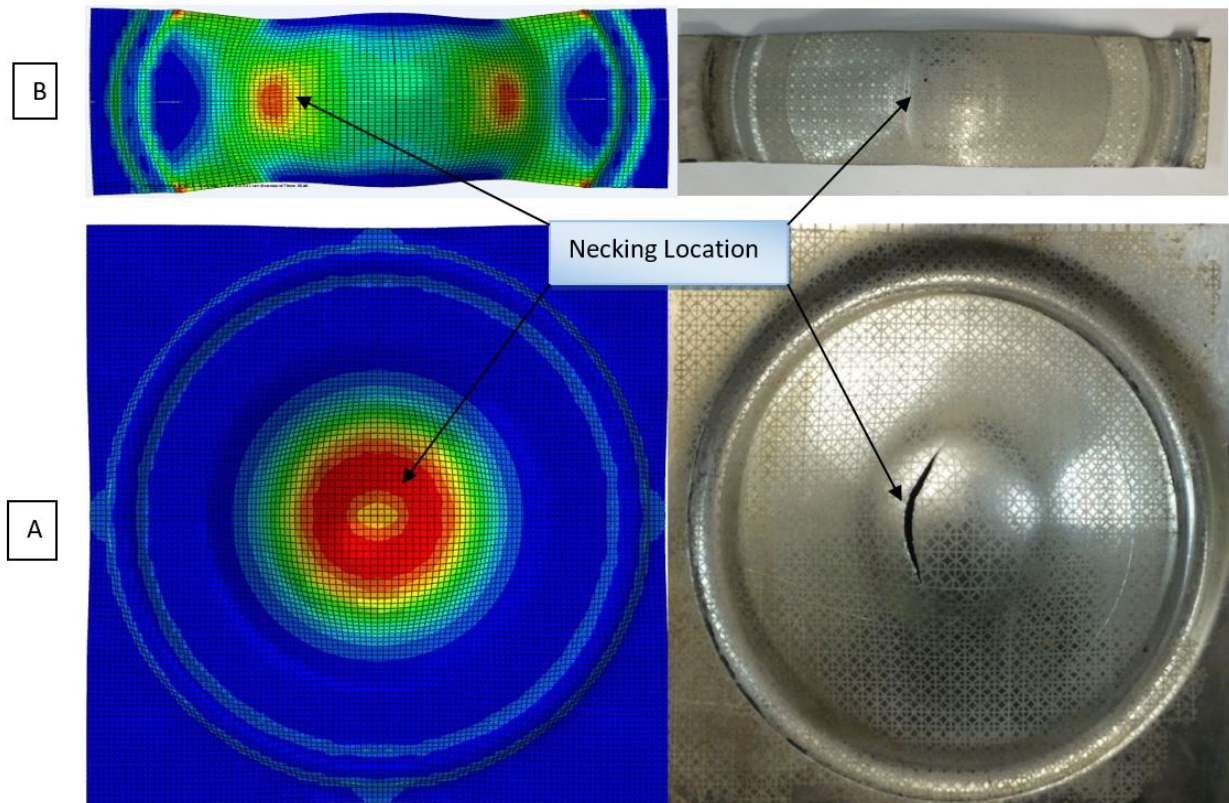
Figure 12: Comparison between tear location in experimental and numerical (second derivative of large strain criterion) at room temperature. A) Biaxial. B) Uniaxial

FLD was drawn using numerical and experimental methods at four temperatures of 25, 150, 200 and 250ºC, in which the numerical part included the Ayada ductile fracture and the maximum large strain acceleration (second derivative (criteria. FLDs for different temperatures are shown in Figures. 13 to 16.
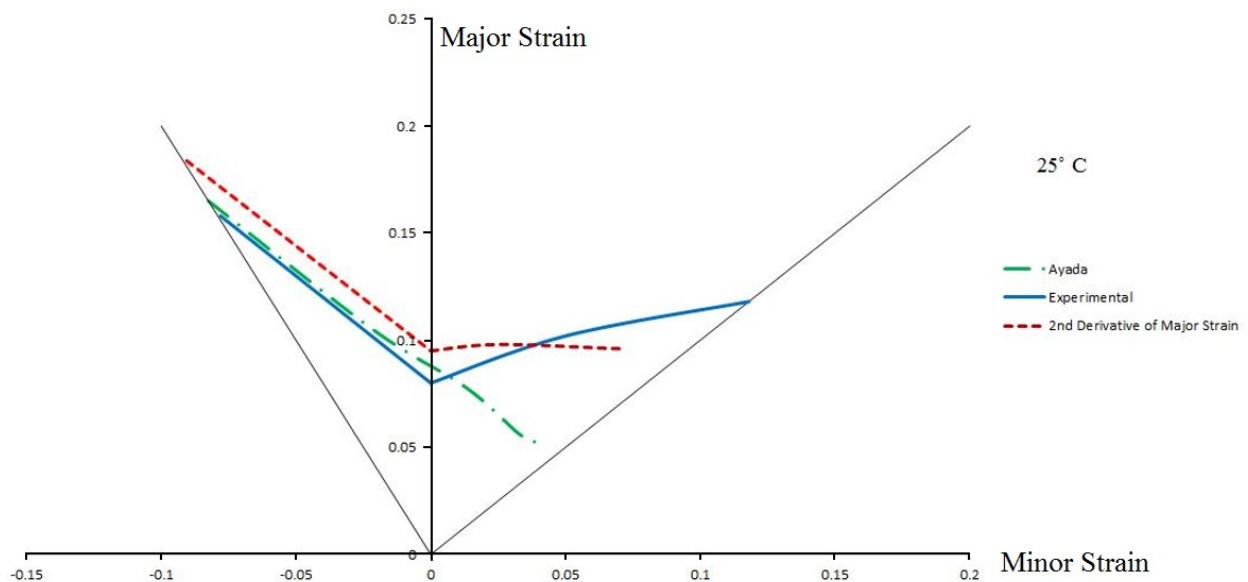

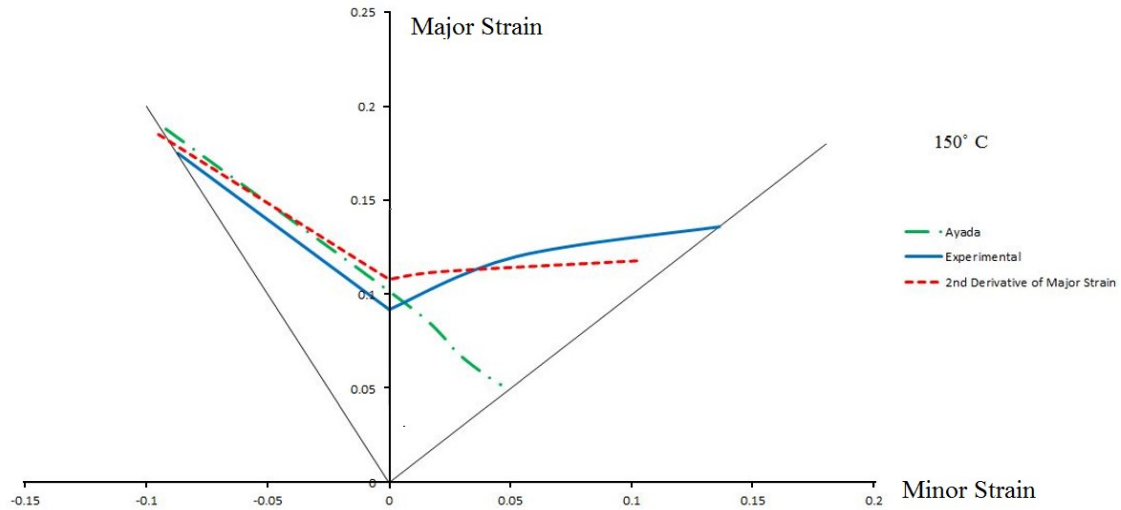
Figure 13: Forming limit diagram at temperature of 25ºC

Numerical and experimental investigation of forming limit diagrams of 6063 aluminum alloy sheets using Ayada ductile fracture criterion and the second derivative of large strain criterion at increased temperatures

Figure 14: *Forming limit diagram at temperature of 150ºC*
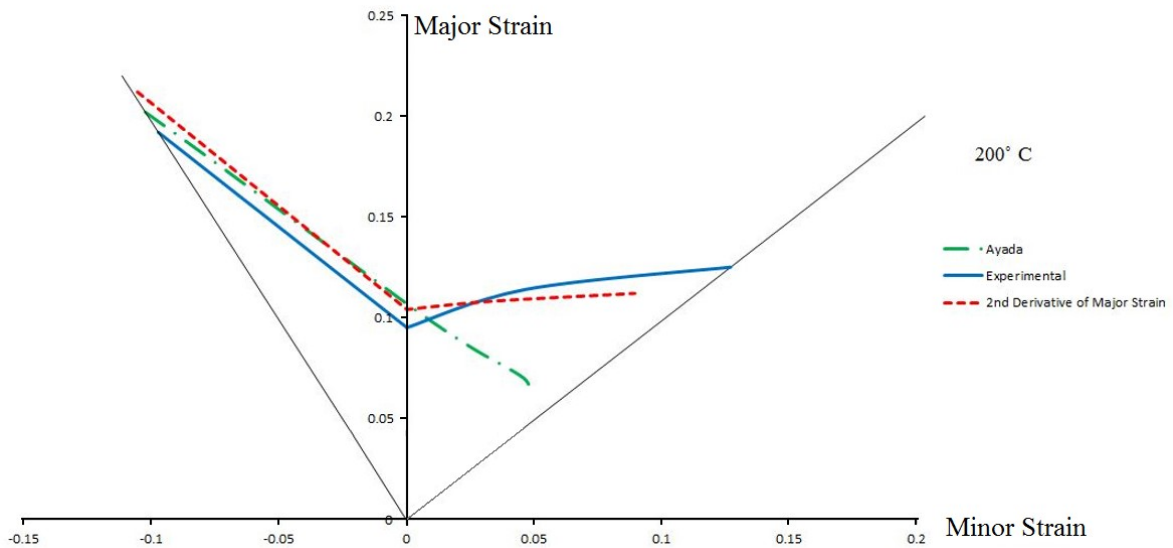
Figure 15: *Forming limit diagram at temperature of 200ºC*

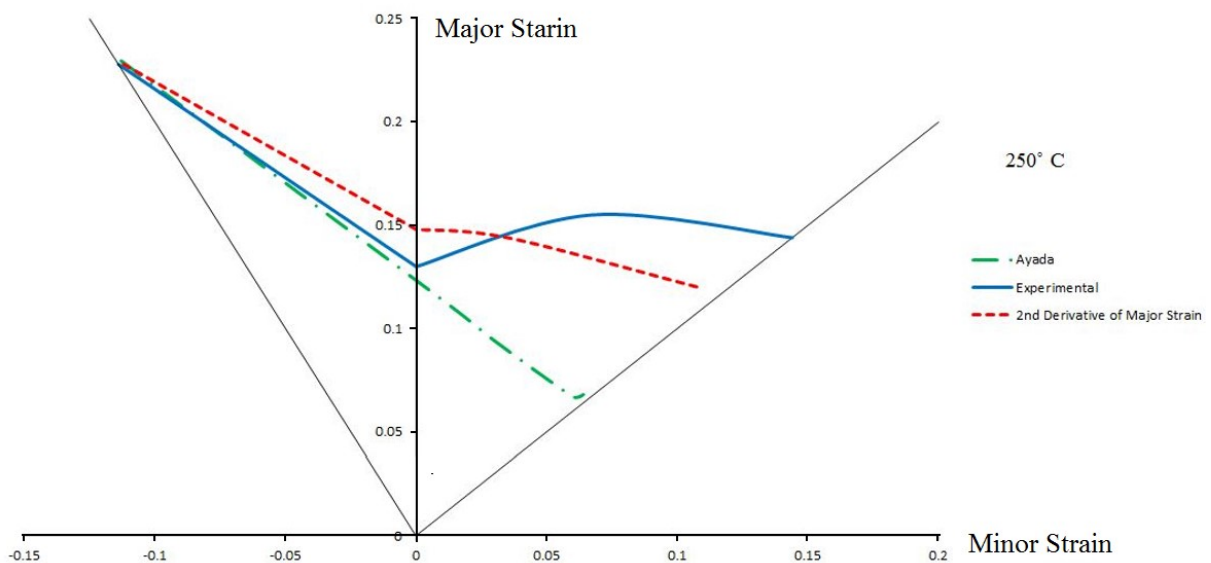**Figure 16:** *Forming limit diagram at temperature of 250ºC*

Alireza Heidari et al.
Numerical and experimental investigation of forming limit diagrams of 6063 aluminum alloy sheets using Ayada ductile fracture criterion
and the second derivative of large strain criterion at increased temperatures

It could be understood that there was a good compatibility between numerical and experimental diagrams. The results also showed that for negative small strains (horizontal axis), the Ayada criterion was more suitable, which was a function of the average stress and the flow stress, while for positive small strains, the second derivative criterion, which depended on the behavior of the large strain over time, was a more suitable criterion.

FLDs resulting from the Ayada criterion in different temperatures show that the diagrams are almost linear and descending; they are closer to a straight line at the left side (in which the minor strain have negative values). In general, in these diagrams, they can be seen that with the increase in the minor strain, the major strain value decrease. According to Figures 13 to 16, with the increase in temperature, the FLD move upward, this fact shows the improvement of formability at higher temperatures.

The experimental FLDs at different temperatures show that diagrams are descending and linear at the left side, but they are ascending at the right side, contrary to the results obtained using the Ayada criterion. The Figures 13 to 16 also show that with the increase in the operational temperature, the formability of the samples increase, so leading to the improved forming limit.

The FLDs were calculated using the second derivative of the major strain criterion at different temperatures show that with the increase in temperature, the forming limit improves. The temperature of 250ºC was found to have a significantly higher formability, as compared to other temperatures.

The increase in formability at elevated temperatures, as compared to room temperature, for each of the investigated criteria in the planar strain conditions can be seen in Table 3. As can be seen, according to the empirical results, Ayada and second derivative criteria, the improvement in the formability of 6063 aluminum alloy sheets was almost equal at the temperatures of 150 and 200ºC, not exceeding 30%, while at the temperature of 250ºC, the improvement in formability ex

ceeded 50%, showing a significant improvement in sheet formability at this temperature.

Table 7: Improvement in sheet formability at different temperatures in planar strain conditions compared to room temperature

Analysis method	150°C	200°C	250°C
Ayada criterion	26%	30%	55%
Experimental test	15%	18%	62%
Second derivative of large strain criterion	13%	10%	55%

The Equation (5) was used to calculate the amount of sheet formability improvement in percentage at elevated temperature according to Table 7 for the plane strain mode:

$$Formability\ Improvement = \frac{\varepsilon_t - \varepsilon_{room}}{\varepsilon_{room}} \times 100 \tag{5}$$

, where ε_t is the plane strain for each of the criteria at the desired temperatures (the position of all the diagrams intersecting in Figures 14-16 with the vertical axis or the same as the major strain axis) and ε_{room} is the plane strain in each of the corresponding criteria at room temperature (the location of each of the intersecting diagrams shown in Figure 13 with the vertical axis or the same as the major strain axis).

6. Conclusion

The present study investigated the FLD of 6063 aluminum alloy sheets by using numerical as well as experimental methods. To estimate the FLD, Ayada and the second derivative of large strain criteria were used. The results showed that numerical diagrams had good compatibility with the experimental results. The results of the Ayad criterion were more compatible for the negative small strains, while the second derivative of large strain was more suitable for the positive small strains.

The results show that the Ayada criterion on the left side of the diagram (negative minor strains) is slightly different from the one obtained by the empirical diagram. But this does not apply to the right, showing a large difference with the Ayada criterion. On the other hand, the diagram resulting from the second derivative criterion on the left side of the diagram does not have much difference, but its compatibility with the empirical diagram on the right side is much more reasonable, as compared to the Ayada criterion. Nevertheless, on the left side of the diagram, the prediction of the FLD according to the Ayada criterion has less error than the second derivative criterion.

Based on the previous research on FLD prediction using ductile fracture criteria, it has been shown that these criteria are very effective in the left side of the diagram, but they are not at all effective at the right; according to the results obtained in the simulation and empirical work, the present research shows that the second derivative criterion is

more appropriate than the ductile fracture criteria, especially the Ayada criterion, in predicting the right side (positive minor strains) of the FLD.

The results also indicated that with the increase in temperature, the FLD moved upward, showing improvement in the formability of alloy sheets. Investigating the amount of improvement in formability for different temperatures showed that the temperature of 250ºC had a significantly better formability in comparison to other temperatures, while formability at 150 and 200 ºC was almost equal. Therefore, the suggestions is that forming operations be carried out at 250 ºC to improve formability by more than 50%.

Appendix A: Abbreviations

FLD	Forming Limit Diagram
FLSD	Forming Limit Stress Diagram
FLC	Forming Limit Curve
LDH	Limit Drawing Height
LDR	Limit Drawing Ratio
M-K	Marciniak-Kuczynski
FEM	Finite Element Method
FE	Finite Element
PEEQ	Equivalent Plastic strain

References

Abedrabbo, N., Pourboghrat, F., and Carsley, J. (2007), Forming of AA5182-O and AA5754-O at elevated temperatures using coupled thermo-mechanical finite element models. International Journal of Plasticity, 23, 841-75.

Allwood, J.M., and Shouler, D.R. (2009), Generalised forming limit diagrams showing increased forming limits with non-planar stress states. International journal of Plasticity, 25, 1207–1230.

Ayada, M., Higashino, T., and Mori, K. (1987), Central bursting in extrusion of inhomogeneous materials", Advanced Technology of Plasticity, 1,553–558.

Bagheriasl, R., Ghavam, K., and Worswick, M.J. (2014), Formability improvement with independent die and punch temperature control, International Journal of Material Forming 7,139-154.

Banabic, D., Comsa, D.S., Jurco, P., Cosovici, G., Paraianu, L., and Julean, D. (2004), FLD theoretical model using a new anisotropic yield criterion. Journal of Materials Processing Technology, 157–158, 23-27.

Bolt, P.J., Lamboo, N.A.P.M., and Rozier, P.J.C.M. (2001), Feasibility of warm drawing of aluminum products" Journal of Materials Processing Technology, 115,118-121

Bressan, J.D., Moreira, L.P., Santos Freitas, M.C., Bruschi, S., Ghiotti, A., and Michieletto, F. (2016), Modelling of Forming Limit Strains of AA5083 Aluminum Sheets at Room and High Temperatures. Advanced Materials Research, Trans Tech Publications, Vol. 1135. 202-217

Brozzo, P., Deluca, B., and Rendina, R., (1972), A new method for the prediction of formability in metal sheets, in: Proceedings of the Seventh Biennial Conference on Sheet Metal Forming and Formability, International Deep Drawing Research Group.

Brun, R., Chambard, A., Lai, M., and De Luca, P. (1999), Actual and virtual testing techniques for a numerical definition of materials. In: Proceedings of NUMISHEET'99, Besanc.on, France, 393–398.

Butuc, M.C., Gracio, J.J., and Barata da Rocha, A. (2003), A theoretical study on forming limit diagrams prediction. Journal of Materials Processing Technology, 142, 714-724

Campos, H.B., Butuc, M.C., Grácio, J.J., Rocha, J.E., and Ferreira Duarte, J. (2006), Theorical and experimental determination of the forming limit diagram for the AISI 304 stainless steel. Journal of Materials Processing Technology, 179.1-3, 56-60.

Dicecco, S., Butcher, C., Worswick, M., Boettcher, E., Chu, E., and Shi, C. (2016), Determination of forming limit diagrams of AA6013-T6 aluminum alloy sheet using a time and position dependent localized necking criterion. IOP Conference Series: Materials Science and Engineering, Vol. 159. No. 1. IOP Publishing.

Geiger, M., and Merklein, M. (2003), Determination of forming limit Diagrams--a new analysis method for characterization of materials formability. Annals of the CIRP 52, 213–216.

Kaya, S., Spampinato, G., and Altan, T. (2008), An Experimental Study on Nonisothermal Deep Drawing Process Using Aluminum and Magnesium Alloys. Journal of Manufacturing Science and Engineering, 130, 1001-1011.

Khan, A.S., and Huang, S. (1995), Continuum Theory of Plasticity. New York: John Wiley & Sons Inc.

Khan, A.S., and Liu, H. (2012), A new approach for ductile fracture prediction on Al 2024-T351 alloy, International Journal of Plasticity, 35, 1–12.

Kim, H.S., Koc, M., Ni, J., and Ghosh, A. (2006), Finite element modeling and analysis of warm forming of aluminum alloys-validation through comparisons with experiments and determination of a failure criterion. Journal of Manufacturing Science and Engineering, 128,613-621.

Li, D., and Ghosh, A.K. (2004), Biaxial warm forming behavior of aluminum sheet alloys. Journal of Materials Processing Technology, 145.3, 281-293.

Liu, H.S., and Fu, M.W. (2014), Prediction and analysis of ductile fracture in sheet metal forming—Part I: A modified Ayada criterion. International journal of damage mechanics, 23.8, 1189-1210.

Min, J., Lin, J., Cao, Y., Bao, W., and Lu, Z. (2010), Effect of necking types of sheet metal on the left-hand side of forming limit diagram. Journal of Materials Processing Technology, 210.8, 1070-1075.

Mitukiewicz, G., Anantheshwara, K., Zhou, G., Mishra, R.K., and Jain, M.K. (2014), A new method of determining forming limit diagram for sheet materials by gas blow forming. Journal of Materials Processing Technology, 214.12, 2960-2970.

Naka, T., and Yoshida, F. (1999), Deep draw ability of type 5083 aluminum–magnesium alloy sheet under various conditions of temperature and forming speed", Journal of Materials Processing Technology, 89-90, 19-23.

Narasimhan, K. (2004), A novel criterion for predicting forming limit strains. In: Ghosh, S., Castro, J.C., Lee, J.K. (Eds.), Materials Processing and Design: Modeling, Simulation and Applications. NUMIFORM 2004 Proceedings of the 8th International Conference on Numerical Methods in Industrial Forming Processes. vol. 2. American Institute of Physics, 850–855.

Ozturk, F., and Lee, D. (2004), Analysis of forming limits using ductile fracture criteria. Journal of Materials Processing Technology, 147.3, 397-404.

Petek, A., Pepelnjak, T., and Kuzman, K. (2005), An improved method for determining forming limit diagram in the digital environment. Journal of Mechanical Engineering, 51,330–345.

Schey, J.A. (1992), Formability determination for production control. Journal of Materials Processing Technology, 32.1-2,207-221.

Shehata, F., Painter, M.J., and Pearce, R. (1978), warm forming of aluminum/magnesium alloy sheet. Journal of Mechanical Working Technology 2,279-291.

Situ, Q., Jain, M.K., and Metzger, D.R. (2011), Determination of forming limit diagrams of sheet materials with a hybrid experimental–numerical approach. International Journal of Mechanical Sciences, 53,707–719.

Alireza Heidari et al.
Numerical and experimental investigation of forming limit diagrams of 6063 aluminum alloy sheets using Ayada ductile fracture criterion
and the second derivative of large strain criterion at increased temperatures

Stoughton, T.B., and Yoon, J.W. (2011), A new approach for failure criterion for sheet metals. International Journal of Plasticity, 27,440–459.

Takuda, H., Mori, K., Fujimoto, H., and Hatta, N. (1996), Prediction of forming limit in deep drawing of Fe/Al laminated composite sheets using ductile fracture criterion. Journal of Materials Processing Technology, 60, 291–296.

Takuda, H., Mori, K., and Hatta, N. (1999), The application of some criteria for ductile fracture to the prediction of the forming limit of sheet metals. Journal of Materials Processing Technology, 95,116–121.

Takuda, H., Mori, K., Masuda, I., Abe, Y., and Matsuo, M. (2002), Finite element simulation of warm deep drawing of aluminum alloy sheet when accounting for heat conduction. Journal of Materials Processing Technology, 120,412-418.

Volk, W. (2006), New experimental and numerical approach in the evaluation of the FLD with the FE-method. In: Proceedings of the FLC-Zurich 06, Zurich, Switzerland.

Wierzbicki, T., Bao, Y., Lee, Y.W., and Bai, Y. (2005), Calibration and evaluation of seven fracture models, International Journal of Mechanical Sciences, 47,719–743.

Wu, P.D., Chen, X.X., Lloyd, D.J., and Embury, J.D. (2009), Effects of superimposed hydrostatic pressure on fracture in sheet metals under tension. International Journal of Mechanical Sciences, 52,236–244.

Xue, L. (2008), Constitutive modeling of void shearing effect in ductile fracture of porous materials. Engineering Fracture Mechanics, 75, 3343–3366.

Yue, Z.M., Badreddine, H., Dang, T., Saanouni, K., and Tekkaya, A.E. (2015), Formability prediction of AL7020 with experimental and numerical failure criteria. Journal of Materials Processing Technology, 218, 80-88.

Zadpoor, A.A., Sinke, J., and Benedictus, R. (2007), Prediction of limit strains in limiting dome height formability test. In: Cueto. E., Chinesta, F. (Eds.), 10th ESAFORM Conference on Material Forming. American Institute of Physics, 258–263.

Zhang, C., Leotoing, L., Guines, D., and Ragneau, E. (2009), Theoretical and numerical study of strain rate influence on AA5083 formability. Journal of materials processing technology, 209.8, 3849-3858.